Determination of the hyperfine structure constants of the ^{87}Rb and ^{85}Rb $4D_{5/2}$ state and the isotope hyperfine anomaly

Jie Wang, Huifeng Liu, Guang Yang, Baodong Yang, and Junmin Wang*

State Key Laboratory of Quantum Optics and Quantum Optics Devices and Institute of Opto-Electronics, Shanxi University, Tai Yuan 030006, Shan Xi Province, People's Republic of China

(Received 2 July 2014; published 10 November 2014)

The hyperfine structure (hfs) splittings of the $4D_{5/2}$ state for two isotopes of ^{87}Rb and ^{85}Rb atoms are measured based on double-resonance optical pumping spectra in a $5S_{1/2}$-$5P_{3/2}$-$4D_{5/2}$ ladder-type atomic system. The frequency calibration is performed by employing a wideband fiber-pigtailed phase-type electro-optic modulator together with a Fabry-Pérot cavity to cancel the error arising from nonlinear frequency scanning. The hfs magnetic dipole constant $\boldsymbol{A}$ of the $4D_{5/2}$ state is determined to be -16.801 ± 0.005 MHz for ^{87}Rb and -4.978 ± 0.004 MHz for ^{85}Rb. The hfs electric quadrupole constant $\boldsymbol{B}$ of the $4D_{5/2}$ state is determined to be 3.645 ± 0.030 MHz for ^{87}Rb and 6.560 ± 0.052 MHz for ^{85}Rb. The values of $\boldsymbol{A}$ and $\boldsymbol{B}$ for the ^{87}Rb $4D_{5/2}$ state are twice as accurate as previous work with thermal atoms using a femtosecond laser comb and the values of $\boldsymbol{A}$ and $\boldsymbol{B}$ for the ^{85}Rb $4D_{5/2}$ state are 3 times and 25 times more accurate than previous work in laser-cooled atoms using Fabry–Pérot interferometer, respectively. According to this high precision of the hfs constants and the previously measured nuclear g factors of the two isotopes, the value of the d-electron hyperfine anomaly $^{87}\Delta^{85}(4D_{5/2})$ is derived to be -0.0041 ± 0.0009.

DOI: 10.1103/PhysRevA.90.052505 PACS number(s): 32.10.Fn, 32.30.−r

I. INTRODUCTION

High-precision measurement of an atomic hyperfine structure (hfs) plays an important role in tests of fundamental physical constants and insights into atomic structure [1,2]. The hfs of alkali-metal atoms has long been a matter of considerable interest because it can be simply modeled as consisting of a single valence electron interacting with a central field generated by the nucleus and core electrons; e.g., Arimondo *et al.* [1] have comprehensively reviewed the experimental investigation. Moreover, the hfs in exited states of alkali-metal atoms provides a stringent testing ground for state-of-the-art atomic calculations based on the best wave functions [3] because it is sensitive to effects such as core polarization and electron correlation. Heavy-alkali-metal atoms are also important in studies of atomic parity, violation, and the search for a permanent atomic electric dipole moment. In these experiments, accurate calculations are needed to properly interpret the experimental results.

The hyperfine anomaly between different isotopes of the same element, arising from the isotope differences in the distribution of nuclear charge and magnetization, is a way of extracting information about nuclear structure such as the configuration interaction or core polarization [4]. In order to determine the hyperfine anomalies, both the nuclear g factors and the magnetic dipole hfs constants have to be experimentally determined with high accuracy. In the review of experimental and theoretical investigations by Büttgenbach [4], the hyperfine anomalies have been determined in a number of isotopes in free atoms by optical and radio-frequency spectroscopy, in paramagnetic systems by electron nuclear double resonance spectroscopy, and in ferromagnetic alloys by nuclear magnetic resonance and perturbed angular correlations techniques. We note that most of those measurements have been done in the ground or metastable states and a very few in excited states. The reason was because the hfs anomalies were as small as $10^{-2}-10^{-4}$. The nuclear g factors could be easily measured with high accuracy ($10^{-4}-10^{-7}$). Also, the magnetic dipole hfs constants for the ground or metastable states could be measured with high accuracy ($10^{-6}-10^{-10}$); however, for the excited states, it is difficult to reach this accuracy mainly due to the weak magnetic dipole interaction and low signal-to-noise ratio (SNR). Experimental approaches such as femtosecond frequency combs and narrow linewidth lasers together with laser cooling and trapping of atoms have achieved increased accuracy for high-precision studies of hfs in excited states [5–7]. Recently, Persson [8] compiled an up-to-date table of experimental values of magnetic hyperfine anomaly in atomic and ionic systems with respect to ground states and a few interesting excited states. In addition, the hyperfine anomaly shows a state dependence, where the values for different states can vary significantly, but shows an n independence, as experimentally found in Rb $S_{1/2}$ and $P_{1/2}$ states [9].

The splitting of hfs due to the electron-nuclear interactions provides information about both the electronic and the nuclear structure of the atoms [10]. For the hfs of S and P states in alkali-metal atoms, the high-precision experimental results agrees well with theoretical predictions; however, the D state remains a significant computational challenge due to strong correlation effects [11]. The excitation from S to D states of alkali-metal atoms cannot be attained by single-photon absorption via the electric dipole transition from the ground state. These spectroscopic forbidden transitions can be satisfied by two-photon transitions [2]. The hfs of D states was investigated by cascade radio-frequency spectroscopy, optical-optical double resonance (OODR), two-photon spectroscopy, and double-resonance optical pumping (DROP) [1,12]. For the hfs constants of the Rb $4D_{5/2}$ state, Liao *et al.* [13] determined the magnetic dipole hfs constants $\boldsymbol{A}$ of ^{87}Rb and ^{85}Rb utilizing cascade radio-frequency spectroscopy, but

*Corresponding author: wwjjmm@sxu.edu.cn

they did not determine the electric quadrupole hfs constant $\boldsymbol{B}$, as the $\boldsymbol{B}$ values were too small to be measured or the SNR was too low. In laser-cooled atoms, Sinclair *et al.* [14] determined the hfs constants $\boldsymbol{A}$ and $\boldsymbol{B}$ of ^{85}Rb utilizing OODR spectroscopy. However, the SNR of OODR is low because the intermediate state with a large spontaneous emission rate is not easily populated in an alkali-metal atomic ladder-type system. Moon *et al.* [15] developed DROP to overcome this limitation. Moreover, with the help of electromagnetically induced transparency (EIT) in a ladder-type atomic system, the linewidth of DROP for counterpropagation is much narrower than that for copropagation [16,17]. Lee *et al.* determined the the hfs constants $\boldsymbol{A}$ and $\boldsymbol{B}$ of ^{87}Rb with a femtosecond frequency comb [18]. Though the optical-frequency comb provides perfect accuracy, it is too complicated and expensive. Fortunately, we are usually concerned with relative frequencies or frequency intervals between hyperfine components. These can be easily performed by optical techniques using an acousto-optic modulator [19], electro-optic modulator (EOM) [20], or a frequency analyzer as a Fabry-Pérot (FP) cavity [21]. However, the error arising from nonlinear frequency scanning is difficult to remove while calibrating the frequency axis.

In this paper we obtained DROP spectra in the $5S_{1/2}$-$5P_{3/2}$-$4D_{5/2}$ system of ^{87}Rb and ^{85}Rb at room temperature and narrowed the linewidth of DROP with the counterpropagation arrangement. The frequency interval calibration of high-resolution DROP spectra was performed using the transmitted peaks through the FP cavity in which the scanning laser was phase modulated using a wideband fiber-pigtailed phase-type EOM. By selecting an appropriate radio frequency that drives the EOM and an appropriate length of cavity, the FP peaks appeared simultaneously with the DROP peaks. Hence the error arising from nonlinear frequency scanning was nearly eliminated [22]. Finally, we measured the hfs splittings of $4D_{5/2}$ in ^{87}Rb and ^{85}Rb atoms and determined the hfs constants $\boldsymbol{A}$ and $\boldsymbol{B}$. The value of d-electron hyperfine anomaly $^{87}\Delta^{85}$ $(4D_{5/2})$ was derived according to the hfs constants of high precision and the previously measured nuclear g factors of the two isotopes.

II. PRINCIPLES

The hfs results from the coupling of the total electron angular momentum $\mathbf{J}$ with the total nuclear angular momentum $\mathbf{I}$. The hyperfine interaction for the electron-nuclear system is represented by the Hamiltonian

$$H_{\rm hfs} = A\mathbf{I}\cdot\mathbf{J} + B\frac{3(\mathbf{I}\cdot\mathbf{J})^2 + \frac{3}{2}(\mathbf{I}\cdot\mathbf{J}) - I(I+1)J(J+1)}{2I(2I-1)J(2J-1)}, \tag{1}$$

where A is the magnetic dipole hfs constant, B is the electric quadrupole hfs constant, I is the nuclear spin angular momentum quantum number, and J is the total electron angular momentum quantum number. Here we have neglected the magnetic octupole hyperfine interaction, which is about four orders of magnitude weaker than the magnetic dipole and electric quadrupole hyperfine interactions [23,24].

The derivation of A for a pointlike atom by Fermi and Segrè assumes a point nuclear magnetic dipole [2]

$$A_{\rm pt} = \frac{16\pi}{3}\frac{\mu_0}{4\pi h} g_I \mu_N \mu_{\rm B} |\psi(0)|^2, \tag{2}$$

where $\psi(0)$ is the electronic wave function evaluated at the nucleus, $\mu_{\rm B}$ is the Bohr magneton, μ_N is the nuclear magneton, and g_I is the nuclear g factor. For an extended nucleus, however, the specific finite electric charge and magnetization distributions have to be taken into account. They cause modifications of A, which are described by

$$A = A_{\rm pt}(1+\varepsilon_{\rm BR})(1+\varepsilon_{\rm BW}), \tag{3}$$

where A denotes the experimental value of the magnetic dipole hfs constant; $\varepsilon_{\rm BR}$ is the modification of the electron wave functions by the extended nuclear charge distribution, the Breit-Rosenthal-Crawford- Schawlow correction [25–27]; and $\varepsilon_{\rm BW}$ is the modification of the finite space distribution of the nuclear magnetization, the Bohr-Weisskopf effect [28].

The hypothetical $A_{\rm pt}$ cannot be calculated with sufficient precision for ordinary (hydrogenlike) atoms, muonic atoms, or hydrogenlike ions. However, these uncertainties in pointlike interactions cancel if we take the ratio of the A values for two isotopes 1 and 2:

$$\frac{A^1_{\rm ex}}{A^2_{\rm ex}} \cong \frac{g^1_I}{g^2_I}(1 + {}^1\Delta^2), \tag{4}$$

with ${}^1\Delta^2 = \varepsilon_{\rm BR}(1) - \varepsilon_{\rm BR}(2) + \varepsilon_{\rm BW}(1) - \varepsilon_{\rm BW}(2)$. Precise values of the hyperfine interaction constant A and independently measured g factors are thus needed to obtain the differential hyperfine anomaly.

Consider our two hydrogenlike isotopes of interest ^{87}Rb and ^{85}Rb. The hyperfine anomaly is

$${}^{87}\Delta^{85} = \frac{A^{87}_{\rm ex}/A^{85}_{\rm ex}}{g^{87}_I/g^{85}_I} - 1. \tag{5}$$

The nuclear g factors were already obtained in previous work [1] with high accuracy, which were $-0.000\,995\,141\,4(10)$ for ^{87}Rb and $-0.000\,293\,640\,0(6)$ for ^{85}Rb and the ratio was 3.388 984(8). To obtain the hyperfine anomaly, the magnetic dipole hfs constants of the Rb isotopes should be determined by measuring the hyperfine splittings from F to $F-1$,

$$\begin{aligned}\Delta E_{\rm hfs}(F \to F-1) &= \Delta E_{\rm hfs}(F) - \Delta E_{\rm hfs}(F-1)\\ &= A_{\rm hfs}F + B_{\rm hfs}\frac{\frac{3}{2}F\left[F^2 - I(I+1) - J(J+1) + \frac{1}{2}\right]}{I(2I-1)J(2J-1)}.\end{aligned} \tag{6}$$

III. EXPERIMENT

There are two naturally occurring isotopes of rubidium: ^{87}Rb with an abundance of 27.8% and ^{85}Rb with an abundance of 72.2%; their nuclear spin angular momentum quantum numbers are 3/2 and 5/2, respectively. Figure 1 shows an energy-level diagram of the $5S_{1/2}$-$5P_{3/2}$-$4D_{5/2}$ transitions of the two isotopes ^{87}Rb and ^{85}Rb. When the frequency of the first laser (L1) is resonant with the cyclical transition of the $5S_{1/2}$-$5P_{3/2}$ transition (the Rb D_2 line), three hfs components of the $4D_{5/2}$ ($F'' = 4,3,2$) line of ^{87}Rb and the $4D_{5/2}$ ($F'' =$

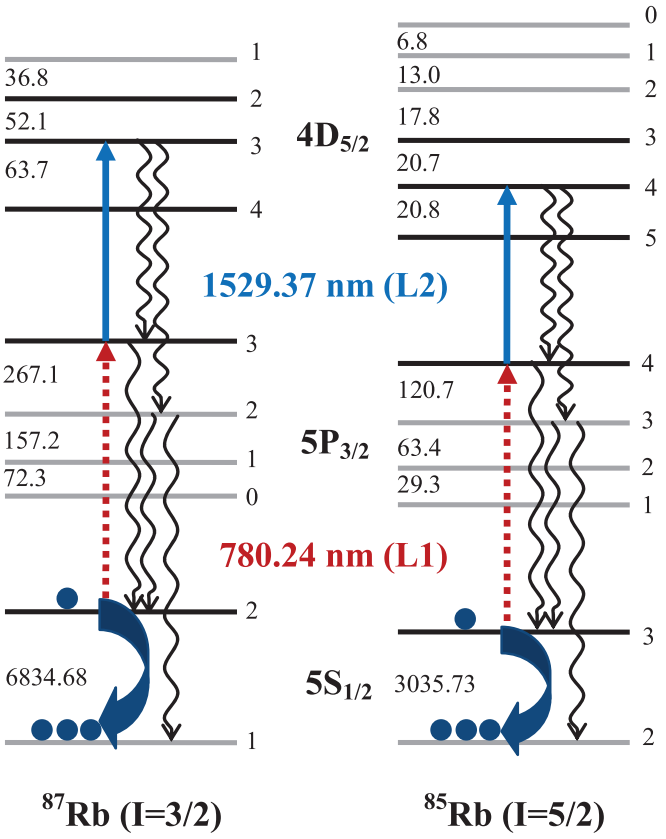

FIG. 1. (Color online) Energy-level diagram of the $5S_{1/2}$-$5P_{3/2}$-$4D_{5/2}$ transitions of two Rb isotopes. The units of hyperfine splittings are MHz.

5,4,3) line of ^{85}Rb can be obtained by the second laser (L2) according to the selection rule. In Fig. 1 the hfs components interacting with two lasers are represented by black lines while the other components are represented by gray lines. The lifetime of the $4D_{5/2}$ state is known to be approximately 84.0 ns (with a linewidth of $2\pi \times 1.89$ MHz) [29].

In general, high-SNR spectra are necessary for a high-precision measurement. The DROP has a high SNR compared with traditional OODR spectra. The transmittance of the DROP spectra can be illustrated by the double-resonance optical pumping from one ground state to another. If we take ^{85}Rb $5S_{1/2}(F = 3)$-$5P_{3/2}(F' = 4)$-$4D_{5/2}(F'' = 4)$ for example, L1 is locked to the $(F = 3)$-$(F' = 4)$ transition, while L2 is tuned to the $(F' = 4)$-$(F'' = 4)$ transition and many atoms in the ground state $F = 3$ are excited to the excited state $F'' = 4$ and then decay to another ground state $F = 2$ through intermediate states $F' = 3$. As a result, the atomic absorption of light becomes weaker due to the reduction of atom population on the ground state $F = 3$. Thus the transmittance signal of L1 is as a function of the detuning of L2. However, the OODR spectra from this system would have a low SNR since there would be only a small population of the intermediate state, which has a large spontaneous emission rate. Thus the DROP spectra are better than the OODR spectra [15]. Similarly, the DROP spectrum of the $(F' = 4)$-$(F'' = 3)$ transition is obtain by the DROP channel through intermediate states $F' = 2,3$.

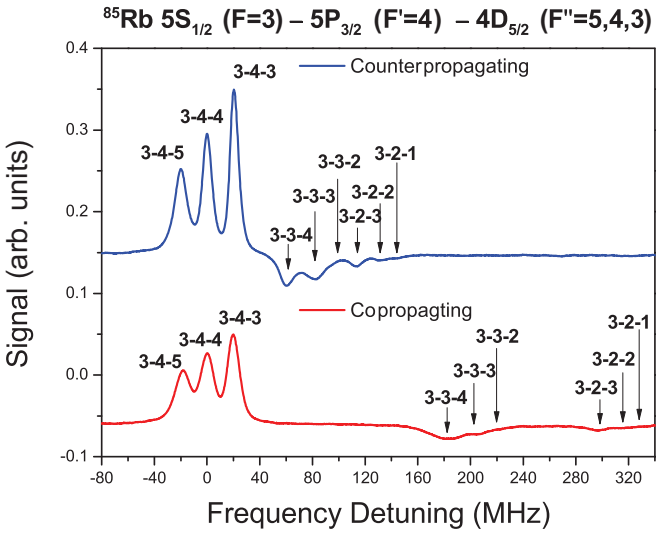

FIG. 2. (Color online) The DROP spectra for counterpropagation and copropagation. The dipole-allowed transition $5S_{1/2}(F = 3)$-$5P_{3/2}(F' = 4)$-$4D_{5/2}(F'' = 5)$ is labeled 3-4-5 and so on. The frequency of 3-4-4 is set as the origin.

Strangely, for the $(F' = 4)$-$(F'' = 5)$ transition, there is not an intermediate-state decay to the other ground state because there are only three states below the $4D_{5/2}$ state [$5S_{1/2}(F = 2,3)$, $5P_{1/2}(F' = 2,3)$, and $5P_{3/2}(F' = 1,2,3,4)$], but there is also transmitted peak, which may be caused by the DROP process through collisional relaxation to the ground state $F = 2$ and quantum interference effects.

A narrow spectral width can improve the resolution of spectroscopy. It not only is of benefit to the determination of the peak centers, but also effectively overcomes the overlap between adjacent spectral lines especially when the distance of the lines is very small. To narrow the linewidth of the DROP spectra, we arrange the two lasers L1 and L2 for counterpropagation (CTP) and copropagation (CP). Figure 2 shows the DROP spectra in the ^{85}Rb $4D_{5/2}$ state for CTP and CP. The powers of the two linearly polarized lasers L1 and L2 are 25 and 90 μW, respectively. Both beam waists are 2 mm and their polarizations are parallel. The linewidth of the DROP spectrum corresponding to the $(F = 3)$-$(F' = 4)$-$(F'' = 3)$ transition for CTP (~7.5 MHz) is narrower than that for CP (~11.5 MHz). This cannot be explained by the EIT due to two-photon coherence in an atomic vapor cell. In an EIT-ladder scheme, the weak probe beam couples the two lower states and the strong-coupling beam the two upper states. For the wavelengths $\lambda_c < \lambda_p$, the EIT effect causes a transmitted peak and with the help of EIT the linewidth of DROP for counterpropagation is much narrower than that for copropagation [16,17]. For the wavelengths $\lambda_c > \lambda_p$, the EIT feature is several orders of magnitude smaller. This occurs because the one-photon Doppler shift $\Delta_{1-\text{pho}} = -k_p v$ has the same sign as the two-photon Doppler shift $\Delta_{2-\text{pho}} = -(k_p - k_c)v$. As a result, the transparency window as a function of detuning no longer exists and adding the contribution from each velocity class strongly reduces the probe transmission peak [30,31]. In our experiment the wavelength of L2 ($\lambda_c = 1529$ nm) is longer than that of L1

($\lambda_p = 780$ nm) and there is no transparency due to EIT. However, the strength of L1 in our experiment is a little stronger and the five-photon term should be included (the EIT is a three-photon term) [32]. The one-photon coherence part due to this high-order term causes the linwidth of CTP to be narrower than that of CP according to Ref. [33]. In short, the DROP experiment with two counterpropagating beams offers a spectrum with a high SNR as well as a narrow linewidth in the $5P_{3/2}$-$4D_{5/2}$ excited-state transition of Rb.

Additionally, the enhanced absorption curves corresponding to $(F = 3)$-$(F' = 3)$-$(F'' = 4,3,2)$ and $(F = 3)$-$(F' = 2)$-$(F'' = 3,2,1)$ channels indicate that the lasers interact with the atoms of different velocity groups due to the Doppler effect. The $(F = 3)$-$(F' = 3)$ transition occurs while atoms move to L1 with velocity $v = \lambda_1\Delta_1$, where Δ_1 is the detuning of L1 and the $(F = 3)$-$(F' = 3)$ transition frequency is for an atom at rest. Hence L2 interacts with this group of atoms. The frequency detunings between the DROP peak 3-4-3 and enhanced absorption 3-3-3 is $\lambda_1/\lambda_2\Delta_1 = (780.24/1529.37)120.7\,\text{MHz} = 61.6\,\text{MHz}$ for CTP and $(\lambda_1/\lambda_2 + 1)\Delta_1 = (780.24/1529.37 + 1)120.7\,\text{MHz} = 182.3\,\text{MHz}$ for CP, which are consistent with Fig. 2.

A. Experimental apparatus

The experimental schematic of the DROP experiment and the hfs splitting measurement is given in Fig. 3. For the DROP experiment, two grating-feedback external cavity diode lasers operating in a single mode are used. As indicated in Fig. 1, the frequency of L1 is fixed on the cyclical $5S_{1/2}$-$5P_{3/2}$ transition of the Rb D_2 line using a modulation lock-in detection

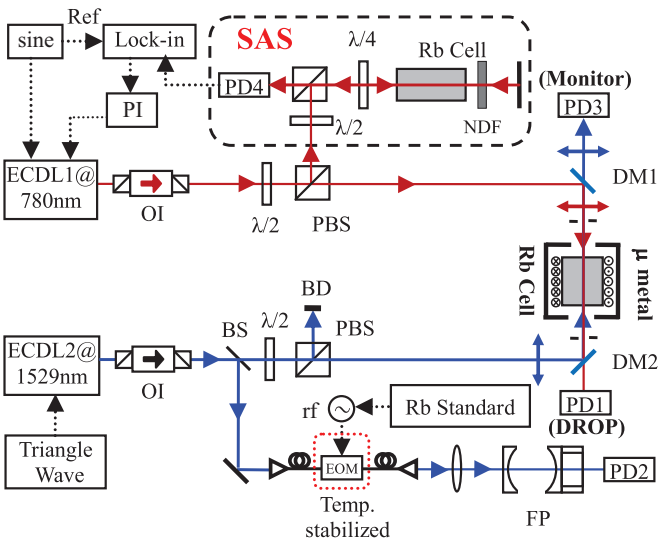

FIG. 3. (Color online) Schematic diagram of the experiment. The following abbreviations are used: sine, sine-wave signal generator; Ref, reference channel of lock-in amplifier; Lock-in, lock-in amplifier; PD, photodiode; SAS, saturated absorption spectroscopy; PI, proportion and integration amplifier; λ/2, half-wave plate; λ/4, quarter-wave plate; NDF, neutral density filter; OI, optical isolator; PBS, polarization beam splitter cube; BS, beam splitter; BD, beam dump; μ metal, magnetic metal; EOM, electro-optic modulator; FP, FP cavity; DM, 45° dichroic mirror; rf, radio frequency signal generator; Rb Standard: Rb frequency standard.

system of saturated absorption spectroscopy. The modulation frequency is 7.8 kHz. To obtain the DROP spectrum in the $5P_{3/2}$-$4D_{5/2}$ transition, the frequency of the second laser diode L2 is scanned over the range of upper states in the $5P_{3/2}$-$4D_{3/2}$ transition and L1 is probed. The optical powers of L1 and L2 entering the Rb cell are measured to be 22 and 86 μW, respectively. The counterpropagating LD1 and LD2 beams are overlapped within 1 mrad using two apertures with a diameter of 2.0 mm. The polarizations of both lasers are linear and parallel to each other in the 5-cm-long Rb vapor cell at room temperature. With a μ-metal magnetic shielding tank around the Rb cell, the residual magnetic field along the axis of the Rb cell is reduced to less than 0.2 mG (20 nT), which is $\sim 10^{-3}$ less than earth's magnetic field (~500 mG). The transmission of L1 through the Rb cell and a dichroic mirror is measured with a photodiode (PD1) to obtain the DROP spectrum. The DROP spectrum is recorded by a digital storage oscilloscope (not shown in Fig. 3). The solenoid coil around the cell, which is placed inside the magnetic shielding tank, is used to examine systematic effects arising from the longitudinal magnetic field. To calibrate the frequency axis, part of the L2 separated from the beam splitter couples to a fiber-pigtailed waveguide-type phase EOM driven by a known radio frequency and is then passed through a FP cavity (with a finesse of ~600 and a free spectral range of ~1.0 GHz) and directed to PD2. The FP signal, including one carrier and two sidebands from PD2, is recorded to calibrate the hyperfine frequency interval of the DROP spectrum.

To eliminate error arising from the nonlinear frequency scanning of L2, we have developed a simple frequency calibration method employing an optical waveguide phase modulator and an FP cavity. First, by scanning the coupling laser's frequency, we obtain the DROP spectra and FP signal from PD1 and PD2, respectively, and simultaneously record the data on a digital storage oscilloscope. Second, we move the FP peak to one of the DROP peaks by adjusting the length of the FP cavity via the voltage driving the piezoelectric actuator. Meanwhile, we use a radio frequency to drive the EOM and set the frequency very close to the DROP peak interval. Thus the FP peaks and the DROP peaks appear simultaneously and the nonlinear error in frequency is eliminated. To reduce systematic error from the calibrator combining the EOM with the FP cavity, we take some appropriate measurements: (i) The large-bandwidth (~10 GHz) EOM, modulated by a radio-frequency signal, has its temperature controlled at (23.00 ± 0.05) °C by a thermoelectric cooler, (ii) the FP cavity is well designed against the thermal fluctuation and mechanical vibration, and (iii) the radio-frequency signal generator is locked to a 10-MHz reference via the rubidium frequency standard with an accuracy of $\pm 5 \times 10^{-11}$ and stability $< 5 \times 10^{-12}$.

B. Experimental results

By scanning the frequency of L2 while fixing L1 to the cyclical transition of the D_2 line, we have recorded the DROP signal and the transmitted signal of the FP cavity from PD1 and PD2 using a digital storage oscilloscope. Typical measurements of the hfs splitting are shown in Fig. 4. The horizontal coordinates are calibrated using a known

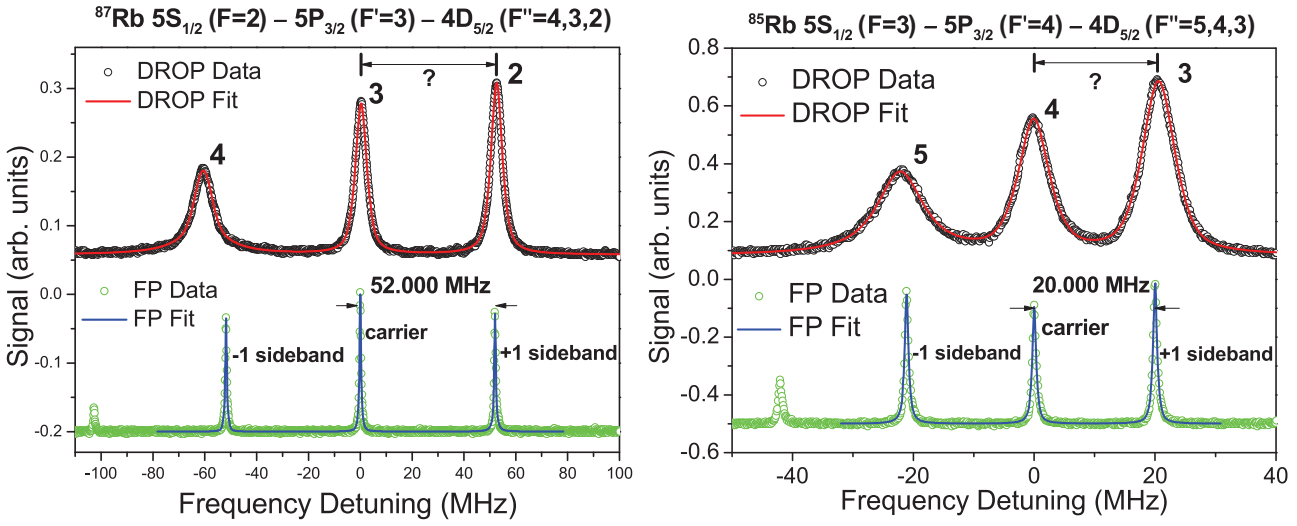

FIG. 4. (Color online) Measurement of the hfs splitting of (a) ^{87}Rb $4D_{5/2}$ ($F'' = 2,3$) and (b) ^{85}Rb $4D_{5/2}$ ($F'' = 3,4$). The upper curve is the DROP experimental data and multipeak Voigt function fit. The linewidth of the noncyclical transition hyperfine components [^{87}Rb $4D_{5/2}$ ($F'' = 2,3$) and ^{85}Rb $4D_{5/2}$ ($F'' = 3,4$)] is about 6 MHz and the linewidth of the cyclical transition hyperfine components [^{87}Rb $4D_{5/2}$ ($F'' = 4$) and ^{85}Rb $4D_{5/2}$ ($F'' = 5$)] is about 9 MHz. The lower curve is the transmission signal of the FP cavity for scanning L2 after the fiber-pigtailed waveguide-type phase modulator. In order to reduce the error arising from the nonlinear frequency scan, the carrier should be placed at one of the DROP peaks. Moreover, the frequency interval between the carrier and sidebands, which are determined by the EOM's driving rf, should be as close as possible to the hfs splitting. The frequency is set to (a) 52.000 MHz, which is close to the hfs splitting between $F'' = 2$ and 3 and (b) 20.000 MHz, which is close to the hfs splitting between $F'' = 3$ and 4. The circles denote the experimental data and the solid line represents the fitted result. Both fitting curves show perfect agreement with the experimental data.

frequency interval between the carrier and sidebands of the FP signal. If we take one of the repeat measurement in Fig. 4(a), for example, to measure the hfs splitting between the ^{87}Rb $4D_{5/2}$, $F'' = 2$ and $F'' = 3$ components, as mentioned above, the carrier of the FP signal is aligned with the $F'' = 3$ DROP peak and then the radio frequency is set to 52.000 MHz, which is very close to the hyperfine interval. Thus the $+1$ sideband is almost adjusted to the $F'' = 2$ DROP peak and the nonlinear error in frequency is eliminated. Moreover, to reduce the systematic errors in calibration, we use two other alignment arrangements that are not shown in Fig. 4: One aligns the carrier with the $F'' = 2$ DROP peak and the -1 sideband with the $F'' = 3$ DROP peak utilizing a 52.000-MHz radio frequency and the other aligns the two sidebands with the two DROP peaks utilizing a 26.000-MHz (half of 52.000 MHz) radio frequency. In each of the three calibration arrangements, we repeat up to 60 times to reduce the statistical error. The measurement of the hfs splitting between ^{87}Rb $4D_{5/2}$, $F'' = 3$ and 4 components is similar, but with a 64.000-MHz radio frequency as reference.

Both the DROP signal and the FP signal are fitted by a multipeak Voigt function to determine the centers of the peaks. The fitting errors (within 95% confidence interval) of the centers range between 5 and 25 kHz for all the DROP data and as low as 2–3 kHz for the FP data. Table I shows the mean values and standard errors of the hfs splittings.

C. Systematic effects

An accurate determination of the hfs splittings requires careful attention to a number of possible systematic uncertainties such as ac Stark shifts, Zeeman shifts, pressure shifts,

TABLE I. Results of the hfs splitting of the Rb isotope $4D_{5/2}$ state including the mean value, standard error, and fitting error based on experimental data for each group of 60 × 3 repeats (in MHz).

Isotope	Hyperfine components	Mean	Standard error	DROP fitting error (mean)	FP fitting error (mean)
^{87}Rb	$(F'' = 3)-(F'' = 2)$	52.044	0.010	0.010 ($F'' = 3$) 0.011 ($F'' = 2$)	0.0025
^{87}Rb	$(F'' = 4)-(F'' = 3)$	64.288	0.016	0.023 ($F'' = 4$) 0.011 ($F'' = 3$)	0.0027
^{85}Rb	$(F'' = 4)-(F'' = 3)$	20.307	0.009	0.008 ($F'' = 4$) 0.006 ($F'' = 3$)	0.0021
^{85}Rb	$(F'' = 5)-(F'' = 4)$	20.955	0.014	0.018 ($F'' = 5$) 0.008 ($F'' = 4$)	0.0020

TABLE II. Error budget for the hfs splittings measurement (in kHz).

Systematic effects	^{87}Rb $F'' = 3$-2	^{87}Rb $F'' = 4$-3	^{85}Rb $F'' = 4$-3	^{85}Rb $F'' = 5$-4
Ac Stark shifts	<4	<4	<4	<4
Zeeman shifts	<0.01	<0.01	<0.01	<0.01
Pressure shifts	<1	<1	<1	<1
Frequency interval calibration	10	21	11	18
Fitting error	15	26	10	20
Total systematic	19	28	15	23
Statistic error	10	16	9	14
Total	21	33	18	27

error arising from misalignment of the CTP laser beams, the locking offset of the probe laser, uncertainty arising from the frequency interval calibration, and fitting error. The associated uncertainties are summarized in Table II and are described in the following.

1. The ac Stark shifts

Theoretically, the ac Stark shifts are almost the same for each hyperfine component of $4D_{5/2}$ and cause no effect on the hyperfine splitting measurement because relative intervals are used. In fact, the hyperfine splittings are slightly different when the optical powers change. For the measurement of hfs splitting between the hyperfine components of the $F'' = 3$ and 2 states of ^{87}Rb, we vary the power of L2, whose intensity is higher, from 0.086 to 1.4 mW. Consequently, we obtain the hfs splitting that depends on the power of L2. We find the slope to be 24(16) kHz/mW, or 2.0(1.4) kHz/I', where I' is the operating intensity 2.7 mW/cm^2. Considering a similar measurement in other hyperfine splittings and the lower intensity of L1, we estimate a maximum uncertainty of 4 kHz at the operating intensity. We take this value as an estimate of the systematic uncertainty from the ac Stark effect.

2. Zeeman shifts

For perfectly linearly polarized laser beams, the residual magnetic field (0.2 mG along the laser beam) due to an imperfect magnetic shield broadens but does not shift the DROP peaks [22]. However, the laser polarization is not perfectly linear in the experiment. To estimate the limit of this effect, we increase the current of the solenoid coil to enlarge the magnetic field and find that the peaks have a broad and even splitting observable for a magnetic field larger than 5 G. We consider that the Zeeman sublevels of $F'' = 3$ and 2 of ^{87}Rb are more sensitive to the magnetic field than other relative hyperfine components because of the large Landé g_F factor [$g_F = 0.60$ for ^{85}Rb ($F = 5,4,3$) components and $g_F = 0.75, 0.85, 1.10$ for ^{87}Rb ($F = 4,3,2$) components, respectively [1]]. We measure the dependence of the hfs splitting between the $F' = 3$ and 2 states of ^{87}Rb on the magnetic field (–0.4 to 0.4 G in steps of 0.1 G) and find a slope of 25(28) kHz/G. Hence the maximum possible uncertainty from the Zeeman shift is less than 0.01 kHz, which is negligible compared with the other uncertainties.

3. Pressure shifts

To estimate the effect of pressure shifts, we monitor the temperature near the Rb vapor cell to be ~22 °C, corresponding to a pressure of 1.1×10^{-6} Torr. Theoretically, the pressure shift is the same for the hyperfine components. In the previous investigation of pressure shift in Rb nD levels impacted by noble gas [34], the pressure shifts are within ±10 kHz for 10^{-6} Torr noble gas. We conservatively estimate that the uncertainty of hyperfine splittings is less than 1 kHz, which is one order of magnitude lower than the probable shift of hyperfine components because the relative intervals are used.

4. Error arising from misalignment of the CTP laser beams

Misalignment of the two beams (<1 mrad) broadens and shifts the peaks through the first-order Doppler shift. Provided the atomic velocity distribution is isotropic, the peaks shift in the same direction equally and their distance remains unchanged. The misalignment, however, can cause a second-order Doppler shift, but it is so small (10^{-1} kHz) that it is negligible [7,35] compared to the other uncertainties.

5. Locking offset of the probe laser

The locking offset of L1 can cause detuning to the resonance transition, but the systematic line shift is negligible because relative intervals are used. Jitter of the laser frequency causes a difference, but as jitter is random, it can be eliminated by repeated measurements.

6. Uncertainty arising from the frequency interval calibration

The possible error from the instability in the frequency interval calibration depends on the nonlinearity in frequency scanning, the thermal fluctuation and mechanical vibration of the FP cavity, and the uncertainty in the radio frequency driving the EOM. Given an appropriate length of cavity and an appropriate radio frequency, the FP peaks appear simultaneously with the DROP peaks. Hence the error arising from nonlinear frequency scanning should be canceled. The instability arising from thermal fluctuations and mechanical vibrations of the FP cavity can be eliminated by making repeated measurements. The radio-frequency signal generator is locked to a rubidium frequency standard with an accuracy of $\pm 5 \times 10^{-11}$ and stability $<5 \times 10^{-12}$, causing an error in the frequency interval calibration of $<10^{-3}$ kHz, which is negligible compared to the FP fitting error. However, the three

kinds of calibration methods make some difference and we take this difference as the uncertainty of frequency calibration.

7. Fitting error

We have used three multipeak profiles (the Gaussian, Lorentzian, and Voigt profiles) to fit the experiment data to determine the centers of peaks. For the DROP peaks, the Lorentzian fit is much better than the Gaussian fit because the DROP is a two-photon process corresponding to the Lorentzian profile [7]. However, a more accurate fit is the multipeak Voigt profile to take into account Doppler broadening effects due to misalignment angle between the two laser beams [36] and perhaps other effects. For FP peaks, the Voigt fit is almost the same as the Lorentz fit. We combine the fitting errors (within 95% confidence interval) for each DROP peak and FP peak in separate hyperfine splittings and get the limit of fitting error in Table II. Finally, combining the total systematic uncertainties with the statistic uncertainties, we obtain the total errors.

D. The hfs constants and hyperfine anomaly

The hfs splittings are written as a function of the magnetic dipole constants and electric quadrupole constants. For the Rb isotope $4D_{5/2}$ state, we calculate them as

$$\begin{aligned}\Delta\nu^{87}[(F''=3)-(F''=2)] &= 3A^{87}-(9B^{87})/20\\ &= -52.044(21)\text{MHz},\\ \Delta\nu^{87}[(F''=4)-(F''=3)] &= 4A^{87}+(4B^{87})/5\\ &= -64.288(33)\text{MHz},\\ \Delta\nu^{85}[(F''=4)-(F''=3)] &= 4A^{85}-(3B^{85})/50\\ &= -20.307(18)\text{MHz},\\ \Delta\nu^{85}[(F''=5)-(F''=4)] &= 5A^{85}+(3B^{85})/5\\ &= -20.955(27)\text{MHz}.\end{aligned}$$

By solving these equations, we obtain the values of A and B listed in Table III. The values of A and B for ^{87}Rb are twice as accurate as previous work with thermal atoms using a femtosecond comb and the values of A and B for ^{85}Rb are, respectively, 3 times and 25 times more accurate than previous work in laser-cooled atoms using FP interferometer.

According to Eq. (5), we derive the hyperfine anomaly $^{87}\Delta^{85}(4D_{5/2})$ to be -0.0041 ± 0.0009. In addition, we have surveyed the hyperfine anomalies of other states and listed them in Table IV. Most of the hyperfine anomalies are calculated from the A values of ^{87}Rb and ^{85}Rb in other works and some of them are directly quoted. Some hyperfine anomalies with big errors are not listed in the table. To be described clearly, we show them in Fig. 5 and find that the hyperfine anomalies of the $S_{1/2}$, $P_{1/2}$, $P_{3/2}$, $D_{3/2}$, and $D_{5/2}$ states show a state dependence, where the values for different states can vary significantly but shows an n independence. This is consistent with the previous experimental extraction in $S_{1/2}$ and $P_{1/2}$ states in Ref. [9].

TABLE IV. Hyperfine anomalies of ^{87}Rb and ^{85}Rb for different levels. The levels in parentheses represent the hyperfine anomalies calculated or directly quoted from other references.

Level	$^{87}\Delta^{85}$	Calculated or directly quoted from
$5S_{1/2}$	-0.00356 ± 0.00008	[1]
$6S_{1/2}$	-0.0036 ± 0.0002	[37]
$7S_{1/2}$	-0.0032 ± 0.0002	[38]
$5P_{1/2}$	-0.0001 ± 0.0001	[39]
$6P_{1/2}$	0.0000 ± 0.0008	[5,6]
$5P_{3/2}$	-0.0005 ± 0.0013	[39]
$(5P_{3/2})$	-0.0002 ± 0.0004	[40,41]
$6P_{3/2}$	-0.0007 ± 0.0016	[1]
$7P_{3/2}$	-0.0002 ± 0.0028	[1]
$4D_{3/2}$	-0.0035 ± 0.0068	[42]
$(4D_{5/2})$	-0.023 ± 0.019	[14,18]
$4D_{5/2}$	-0.0041 ± 0.0009	this work
$5D_{5/2}$	-0.0044 ± 0.0005	[43,44]
$(5D_{5/2})$	-0.001 ± 0.037	[19]

IV. CONCLUSION

In conclusion, we have demonstrated a technique for high-resolution hyperfine splitting measurement in atomic excited states by using DROP in the ladder-type $5S_{1/2}$-$5P_{3/2}$-$4D_{5/2}$ atomic system in a ^{87}Rb-^{85}Rb mixed vapor cell around room temperature. With the help of a one-photon coherence part due to this high-order term in the strong probe regime in the EIT-ladder scheme, the linewidth of DROP for counterpropagation is narrower than that for copropagation, which benefits the determination of the centers of peaks. The frequency axis was calibrated by using a temperature-controlled EOM and a stable FP cavity to reduce the systematic errors. The EOM was modulated by a signal generator (locked to a rubidium frequency standard) with known frequency.

In this manner, we were able to measure hyperfine intervals in the $4D_{5/2}$ state of ^{87}Rb and ^{85}Rb and then determine the hfs constants. The accuracy of A and B for ^{87}Rb is twice as good as previous work with thermal atoms using a femtosecond comb and the accuracy of A and B for ^{85}Rb is, respectively, 3 and 25 better than previous work in laser-cooled atoms using FP interferometer. Finally, by combining the previous

TABLE III. The hfs constants of the $4D_{5/2}$ state of ^{87}Rb and ^{85}Rb isotopes (in MHz). The following types of measurement were used: cascade radiofrequency (cascade rf), femtosecond laser comb (fs comb), FP interferometer, and FP cavity with EOM.

A^{87}	A^{85}	B^{87}	B^{85}	Sample	Type of measurement	Ref.
-16.9 ± 0.6	-5.2 ± 0.3			thermal atoms	cascade rf	[13]
-16.747 ± 0.010		4.149 ± 0.059		thermal atoms	fs comb	[18]
	-5.06 ± 0.10		7.42 ± 0.15	laser-cooled atoms	FP interferometer	[14]
-16.801 ± 0.005	-4.978 ± 0.004	3.645 ± 0.030	6.560 ± 0.052	thermal atoms	FP cavity with EOM	this work

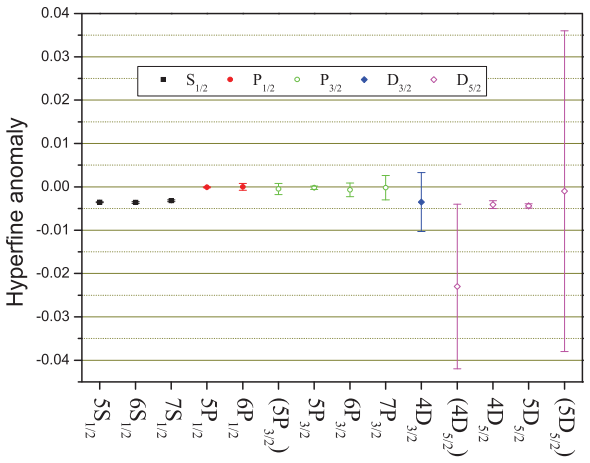

FIG. 5. (Color online) Comparison of the experimental results for the hyperfine anomaly $^{87}\Delta^{85}$.

high-precision measurement of nuclear g factors of the two isotopes, we obtained the d-electron hyperfine anomaly $^{87}\Delta^{85}$ $(4D_{5/2})$. In addition, we experimentally verified that the hyperfine anomaly is state dependent and n independent in the $P_{3/2}$ and $D_{5/2}$ states, which is consistent with the experiments in $S_{1/2}$ and $P_{1/2}$. We believe that this work provides experimental evidence for many-body refinements that strongly perturb the hyperfine interaction such as polarization of the inner electron core, electron correlation, and relativistic effects. Also, this work provides a simple method to measure excited-state hfs in heavy atoms that are of interest for parity nonconserving measurements.

ACKNOWLEDGMENTS

This work was supported by the National Major Scientific Research Program of China (Grant No. 2012CB921601), the National Natural Science Foundation of China (Grant Nos. 11274213, 11104172, 61078051, and 61227902), the Project for Excellent Research Team of the National Natural Science Foundation of China (Grant No. 61121064), the Shanxi Scholarship Council of China (Grant No. 2012-015), and Research Program for Science and Technology Star of Taiyuan, Shanxi, China (Grant No. 12024707).

[1] E. Arimondo, M. Inguscio, and P. Violino, Rev. Mod. Phys. **49**, 31 (1977).
[2] C. J. Foot, *Atomic Physics* (Oxford University Press, Oxford, 2005).
[3] M. S. Safronova, W. R. Johnson, and A. Derevianko, Phys. Rev. A **60**, 4476 (1999).
[4] C. Büttgenbach, Hyperfine Interact. **20**, 1 (1984).
[5] A. Marian, M. C. Stowe, J. R. Lawall, D. Felinto, and J. Ye, Science **306**, 2063 (2004).
[6] A. Marian, M. C. Stowe, D. Felinto, and J. Ye, Phys. Rev. Lett. **95**, 023001 (2005).
[7] J. E. Stalnaker, V. Mbele, V. Gerginov, T. M. Fortier, S. A. Diddams, L. Hollberg, and C. E. Tanner, Phys. Rev. A **81**, 043840 (2010).
[8] J. R. Persson, At. Data Nucl. Data Tables **99**, 62 (2013).
[9] A. Pérez Galván, Y. Zhao, L. A. Orozco, E. Gómez, F. J. Baumer, A. D. Lange, and G. D. Sprouse, Phys. Lett. B **655**, 114 (2007).
[10] V. Gerginov, A. Derevianko, and C. E. Tanner, Phys. Rev. Lett. **91**, 072501 (2003).
[11] V. A. Dzuba, V. V. Flambaum, and J. S. M. Ginges, Phys. Rev. A **63**, 062101 (2001).
[12] W. Demtröder, *Laser Spectroscopy* (Springer, New York, 1998).
[13] K. H. Liao, L. K. Lam, R. Gupta, and W. Happer, Phys. Rev. Lett. **32**, 1340 (1974).
[14] A. G. Sinclair, B. D. McDonald, E. Riis, and G. Duxbury, Opt. Commun. **106**, 207 (1994).
[15] H. S. Moon, W. K. Lee, L. Lee, and J. B. Kim, Appl. Phys. Lett. **85**, 3965 (2004).
[16] H. S. Moon, L. Lee, and J. B. Kim, J. Opt. Soc. Am. B **24**, 2157 (2007).
[17] B. D. Yang, Q. B. Liang, J. He, T. C. Zhang, and J. M. Wang, Phys. Rev. A **81**, 043803 (2010).
[18] W. K. Lee, H. S. Moon, and H. S. Suh, Opt. Lett. **32**, 2810 (2007).
[19] T. T. Grove, V. Sanchez-Villicana, B. C. Duncan, S. Maleki, and P. L. Gould, Phys. Scr. **52**, 271 (1995).
[20] Y. C. Lee, Y. H. Chang, Y. Y. Chang, Y. Y. Chen, C. C. Tsai, and H. C. Chui, Appl. Phys. B **105**, 391 (2011).
[21] S. L. Gilbert, R. N. Watts, and C. E. Wieman, Phys. Rev. A **27**, 581 (1983).
[22] J. Wang, H. F. Liu, B. D. Yang, J. He, and J. M. Wang, Meas. Sci. Technol. **25**, 035501 (2014).
[23] W. G. Jin, M. Wakasugi, and T. T. Inamura, Phys. Rev. A **52**, 157 (1995).
[24] N. C. Lewty, B. L. Chuah, R. Cazan, B. K. Sahoo, and M. D. Barrett, Opt. Express **20**, 21379 (2012).
[25] E. Rosenthal and G. Breit, Phys. Rev. **41**, 459 (1932).
[26] M. Crawford and A. Schawlow, Phys. Rev. **76**, 1310 (1949).
[27] H. J. Rosenberg and H. H. Stroke, Phys. Rev. A **5**, 1992 (1972).
[28] A. Bohr and V. F. Weisskopf, Phys. Rev. **77**, 94 (1950).
[29] O. S. Heavens, J. Opt. Soc. Am. **51**, 1058 (1961).
[30] H. S. Moon and H. R. Noh, J. Opt. Soc. Am. B **29**, 1557 (2012).
[31] A. Urvoy, C. Carr, R. Ritter, C. S. Adams, K. J. Weatherill, and R. Löw, J. Phys. B **46**, 245001 (2013).
[32] S. Wielandy and A. L. Gaeta, Phys. Rev. A **58**, 2500 (1998).
[33] H. R. Noh and H. S. Moon, Opt. Express **19**, 11128 (2011).
[34] K. H. Weber and K. Niemax, Z. Phys. A **307**, 13 (1982).
[35] P. V. Kiran Kumar, M. Sankari, and M. V. Suryanarayana, Phys. Rev. A **87**, 012503 (2013).
[36] K. Pandey, P. V. Kiran Kumar, M. V. Suryanarayana, and V. Natarajan, Opt. Lett. **33**, 1675 (2008).
[37] A. Pérez Galván, Y. Zhao, and L. A. Orozco, Phys. Rev. A **78**, 012502 (2008).
[38] H. C. Chui, M. S. Ko, Y. W. Liu, J. T. Shy, J. L. Peng, and H. Ahn, Opt. Lett. **30**, 842 (2005).

[39] G. P. Barwood, P. Gill, and W. R. C. Rowley, Appl. Phys. B **53**, 142 (1991).
[40] J. Ye, S. Swartz, P. Jungner, and J. L. Hall, Opt. Lett. **21**, 1280 (1996).
[41] A. Banerjee, D. Das, and V. Natarajan, Europhys. Lett. **65**, 172 (2004).
[42] H. S. Moon, W. K. Lee, and H. S. Suh, Phys. Rev. A **79**, 062503 (2009).
[43] F. Nez and F. Biraben, Opt. Commun. **102**, 432 (1993).
[44] F. Nez, F. Biraben, R. Felder, and Y. Millerioux, Opt. Commun. **110**, 731 (1994).